Applied Thermal Engineering 73 (2014) 333–340

Contents lists available at ScienceDirect

Applied Thermal Engineering

journal homepage: www.elsevier.com/locate/apthermeng

Estimation of thermoelectric and mechanical performances of segmented thermoelectric generators under optimal operating conditions

Xiaodong Jia, Yuanwen Gao*

Key Laboratory of Mechanics on Environment and Disaster in Western China, The Ministry of Education of China, and Department of Mechanics and Engineering Sciences, College of Civil Engineering and Mechanics, Lanzhou University, Lanzhou 730000, PR China

HIGHLIGHTS

- The temperature dependent properties of TE materials are taken into account.
- The conversion efficiency can be enhanced by employing the segmented TE materials.
- The operating conditions satisfy the mechanical strength and efficiency requirements.

ARTICLE INFO

Article history:
Received 24 February 2014
Accepted 27 July 2014
Available online 6 August 2014

Keywords:
Conversion efficiency
Mechanical performance
Segmented thermoelectric generator
Optimal operating condition

ABSTRACT

The conversion efficiency is the most important indicator describing the thermoelectric performance of thermoelectric (TE) devices. Under large operating temperature difference, the efficiency can be enhanced by the fabrication of segmented thermoelements structure. For running safety, the thermo-mechanical behavior of TE devices must be considered. In this paper, a 3D finite element model is established to estimate the TE and mechanical performance of the segmented thermoelectric generator (STEG) under optimal operating conditions. The effects of the segment lengths on the TE conversion efficiency and the maximum stress level of TE materials are examined at a given operating temperature. And for different operating temperatures, the maximum conversion efficiency and maximum stress level of TE materials are also investigated, individually. By the mechanical strength evaluation and mechanical reliability analysis, the TE behaviors of STEG are verified. The results indicate that, for a given operating temperature, some segmented cases do not satisfy the strength requirements, and the theoretical maximum efficiency does not equal to the actual optimal one; for different operating temperatures, the STEG cannot always achieve the maximum design value of conversion efficiency. These findings will have some significant positive impact on the optimal design and practical application of the STEG.

1. Introduction

Thermoelectric (TE) technique is a new type of environmentally friendly energy conversion technology, which can realize the conversion between thermal energy and electric energy in the most direct way (i.e. electron transport) by thermoelectric materials [1]. The power devices based on TE materials have many significant applications in military, medical treatment, communication, and space flight and aviation, due to their unique advantages including no working medium leaking and mechanical movement, no vibration and noise, small volume, light weight, and low maintenance cost [2–4].

For TE devices, the conversion efficiency is the key index to evaluate the TE performance. To improve the efficiency, in addition to using high-quality TE materials, the optimal design of the device's structure can be carried out. Jang et al. [5] investigated the influences of the structure parameters on the TE performance of micro-thermoelectric generators by a finite element method. Numerical results indicated that the larger length of the thermoelements corresponds to the higher TE conversion efficiency. And the efficiency increases as the cross-sectional area of the thermoelements reduces. Sahin and Yilbas [6] studied theoretically the effect of the shape parameter, associated with the TE leg geometry, on the conversion efficiency of the TE power generators. Their results

* Corresponding author.
E-mail address: ywgao@lzu.edu.cn (Y. Gao).

http://dx.doi.org/10.1016/j.applthermaleng.2014.07.069
1359-4311/

showed that changing of the shape parameter has a very significant influence on the conversion efficiency. Chen et al. [7] analyzed the TE behavior of the two-stage TE generator, and found that for the fixed total TE elements, the ratio of number of TE elements of the top stage to the total number of TE elements have an optimal value with the highest TE efficiency. For the case of operating at a large temperature difference, the fabrication of segmented thermoelements structure for generator is one of the effective and feasible methods to achieve the higher TE efficiency. Kuznetsov et al. [8] calculated the conversion efficiency of functionally graded and segmented Bi_2Te_3-based thermocouple. It can be found that the conversion efficiency is about 10% which exceeds that of homogeneous Bi_2Te_3-based thermocouple. Vikhor and Anatychuk [9] designed the TE modules of segmented thermoelements based on the optimal control theory, and described the fact that the efficiency of the modules can be more significantly improved by using the two-segmented thermoelements compared with the traditional BiTe material generators. Reddy et al. [10] studied numerically the TE performance of a composite TE device comprised of segmented thermoelements. Their results indicated that the composite TE device shows a 24.8%, 26.2%, and 29.9% increase in conversion efficiency as compared to a conventional TE device when the hot surface temperature T_h = 550 K, 450 K and 350 K respectively.

In practice, TE devices are applied in certain temperature environments. The thermal stress, caused by temperature gradient and thermal expansion mismatch among various components of TE devices, will affect the security service of TE devices. It is therefore essential to consider the influence of mechanical performance when evaluating the TE devices. During the last few years, there are some research works having focused on the mechanical behaviors of TE devices. Clin et al. [11] simulated numerically the thermomechanical behavior of Bismuth-Telluride TE module. Their results indicated that the stress level increases with the length of the TE leg decreasing. Besides, the boundary condition of TE devices and mechanical strength of soldering alloy have some significant effects on the stress distribution in TE elements. Turenne et al. [12] further investigated the thermomechanical characteristics of Bismuth-Telluride TE generators. Numerical results demonstrated that the plastic deformation of soldering materials can effectively reduce the stress value of TE legs. The shorter distance from the TE leg to the edge of the module renders, the higher the maximum stress level in the leg. Al-Merbati et al. [13] discussed the influence of device pin geometry on the thermal stress of TE power generator. They showed that changing the pin geometry can improve the temperature variation in TE device and reduce the maximum stress levels in the TE legs, and thus improve the service reliability. Li et al. [14] investigated the effect of the copper pad thickness on thermomechanical performance of TE modules. Numerical results indicated that for the whole device, the maximum stress level is located on the contact surface between the AlN substrate and the top copper pad because there corresponds to a larger mismatch in thermal expansion coefficients. Under the same temperature difference the thicker the pad thickness is, the higher the maximum Von Mises stress is. The researches on TE and mechanical performance have also been reported. Chen et al. [15] carried out a numerical simulation on the thermal-mechanical-electrical behavior of TE devices based on the actual working environments. Gao et al. [16] investigated the relationship between the thermal stress and the structure parameters of TE leg for a Bi_2Te_3-based TE module, and proposed the optimal lengths of leg and side to improve the conversion efficiency and the stability of the TE module. It can be seen that the research work focuses on homogeneous TE materials devices. To the authors' knowledge, up to now there have been few studies conducted to investigate the mechanical behaviors of segmented thermoelectric generator (STEG) and to guide the structure design by analyzing the mechanical reliability.

In this paper, a 3D finite element model of STEG is established to analyze the TE and thermomechanical behaviors of device under optimal operating conditions. First, based on thermal-electric coupling calculation, the TE conversion efficiency under a given operating temperature is optimized by selecting the appropriate segmented material length. And for different operating temperatures, the theoretical maximum conversion efficiency is also discussed. Then, the thermal-structure coupling calculation is performed and the maximum stress levels of TE materials are obtained under different operating conditions. By the mechanical strength evaluation and mechanical reliability analysis, we investigate the rationality of various segmentation case for a given temperature condition and point out the actual optimal efficiency as well as the corresponding segmentation scheme. For the given operating temperature range, the effective temperature point is also determined, in which not only can the strength requirements be satisfied but also a good efficiency can be produced.

2. Calculation model

2.1. Constitutive equations of thermal-electric and thermal-structural couplings

The geometry model of segmented thermoelectric generator established in this paper is shown in Fig. 1. The STEG is comprised of segmented TE materials, welding strips, conductors and substrates. And the dimensions of the STEG components are listed in Table 1. When a temperature difference is imposed between the up and down substrates, holes in p-type TE material and electrons in n-type TE material are transported from the hot end to cold end, a TE potential difference will be generated at cold sides of thermoelements due to the Seebeck effect. Once the circuit across the thermoelements is closed by a load resistance, there is a direct current flowing through the device. This is the process that TE materials convert thermal energy into electrical energy directly through the temperature difference at the ends of TE device. The process is also accompanied by the Peltier effect, Thomson effect and irreversible Joule and Fourier effects at the same time. Thus, the power generation capacity should be determined by the combination of these effects. The governing equation of heat flow can be expressed as [17].

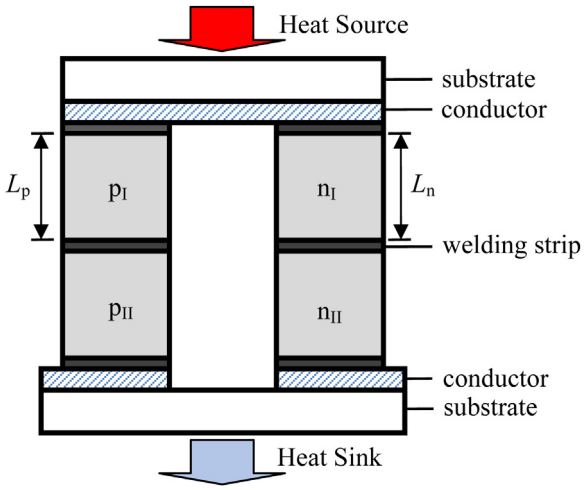

Fig. 1. Structure of the STEG.

Table 1
Dimensions of the STEG components.

Components	Dimensions
Top substrate	15 mm × 5 mm × 2 mm
Bottom substrate	17 mm × 5 mm × 2 mm
TE leg	5 mm × 5 mm × 10 mm
Welding strip	5 mm × 5 mm × 0.5 mm
Top conductor	15 mm × 5 mm × 1 mm
Bottom conductor	6 mm × 5 mm × 1 mm

$$\rho C\frac{\partial T}{\partial t}+\nabla\cdot\mathbf{q}=\dot{q} \tag{1}$$

where ρ is the density, C is the specific heat capacity, T is the absolute temperature, $\dot{q}$ is the heat generation rate per unit volume which stands for an internal heat source and $\mathbf{q}$ is the heat flux vector. The equation of continuity of electric charge can be expressed as [5]

$$\nabla\cdot\mathbf{J}=0 \tag{2}$$

where $\mathbf{J}$ is the electric current density vector. The coupled thermal-electric constitutive equations governing TE phenomena can be expressed as

$$\mathbf{q}=\left[\prod\right]\mathbf{J}-[\lambda]\nabla T \tag{3}$$

$$\mathbf{J}=[\sigma](\mathbf{E}-[\alpha]\nabla T) \tag{4}$$

where $[\prod]=T[\alpha]$ is the Peltier coefficient matrix and $\mathbf{E}$ is the electric field intensity vector. Here, $[\alpha]$, $[\lambda]$ and $[\sigma]$ are dependent with the temperature, which stand for the Seebeck coefficient matrix, thermal conductivity matrix and electrical conductivity matrix, respectively. The electric field is derived form an electric potential φ, expressed by

$$\mathbf{E}=-\nabla\varphi \tag{5}$$

In the TE analysis, the internal heat source $\dot{q}$ includes the electric power spent on Joule heating and on work against the Seebeck field [17], and which can be expressed as.

$$\dot{q}=\mathbf{J}\cdot\mathbf{E} \tag{6}$$

Based on Eqs. (1)–(6), we can easily build the coupled thermal-electric governing equations including the temperature and electric potential.

In accordance with the temperature gradient on the device, the thermal stress is generated in the STEG due to different thermal expansions of various components. The differential equilibrium and strain-displacement equations for the structure can be expressed as.

$$[A]\mathbf{S}+\bar{\mathbf{f}}=\mathbf{0} \tag{7}$$

$$\boldsymbol{\varepsilon}=[A]^{\mathrm{T}}\mathbf{u} \tag{8}$$

where $[A]$ is the differential operator describing the mechanical equilibrium, $\mathbf{S}$ and $\boldsymbol{\varepsilon}$ are respectively the stress vector and strain vector, $\bar{\mathbf{f}}$ is the volume force, and $\mathbf{u}$ is the displacement vector. The coupled thermal-structure constitutive equations can be expressed as [18]

$$\mathbf{S}=[D]\boldsymbol{\varepsilon}-\boldsymbol{\beta}\Delta T \tag{9}$$

$$Q=T_0\boldsymbol{\beta}^{\mathrm{T}}\boldsymbol{\varepsilon}+\rho C_{\mathrm{V}}\Delta T \tag{10}$$

where $[D]$ is the stiffness matrix, $\boldsymbol{\beta}=[D]\mathbf{a}$ is the vector of thermo-elastic coefficients, and $\mathbf{a}$ is the vector of thermal expansion coefficient. Q is the heat density, T_0 is the absolute reference temperature and C_{V} is the specific heat at constant volume. According to Eqs. (1) and (7)–(10) one can formulate the coupled thermal-structure governing equations for the temperature and displacement.

The above equations describe the thermal-electric and thermal-structural couplings and the thermal, electrical and mechanical behaviors of TE devices. The temperature, electric potential and stress can be obtained by solving the couple thermal-electric and thermal-structure governing equations. However, it is very difficult to find the analytical solutions due to the nonlinear temperature-dependent material properties. In this paper, the corresponding finite element equations can be constructed by applying the variation principle on these equations.

2.2. Basic assumptions and boundary conditions

To simplify the calculation model, the interfacial thermal and electrical resistances as well as the heat losses due to heat convection and radiation are neglected. And the heat source and the heat sink are treated as thermal boundary conditions. T_{h} is set on the top substrate of the STEG and the bottom side is kept at T_{c}. The electrical potential at the electrode connected to the cold end of p-leg is zero. In the thermal stress analysis, the STEG is free for deformation under operation.

2.3. Finite element model of the STEG

The component materials of TE device differ from one another: ceramic, copper and Sn–Sb alloy are chosen for the substrates, conductors and welding strip, respectively. The p- and n-type TE legs consist of a hot segment material I (Skutterudite-based material) [19] and a cold segment material II (Bismuth-Telluride-based material), respectively [20]. Here, the ceramic substrate and the TE materials are considered to be brittle materials. The copper strip and the welding strip are regarded as elastoplastic ones. And the yield strength, ultimate strength and the extensibility of the copper strip are specified for 70 MPa, 250 Mpa and 69%. For the welding strip, these values are 26 MPa, 41 MPa and 38%, respectively [16]. For numerical simulation, Table 2 shows thermal-electric and thermal-structure properties of the materials.

The ANSYS software is then used to solve the finite element equations under steady-state conditions and simulate the thermoelectric and thermomechanical behaviors of STEG. Fig. 2 shows a 3D finite element model of STEG. And the distance between adjacent nodes of mesh is 1 mm. For the TE device, the 20-node hexahedral coupling element SOLID226 with five degrees of freedom per node is selected (including temperature, voltage and three displacement components). The general circuit element CIRCU124 with a voltage degree of freedom at per node is used to describe the load resistance R_0. The iterative calculations are performed until the convergence criterions of temperature, voltage and displacement are met.

From the thermal-electric coupling calculation, the heat inputted on the top substrate of the STEG Q_{in} and the power generated in load resistance P at different operating conditions can be determined directly. Then, the TE conversion efficiency of the STEG can be obtained by [5].

Table 2
Properties of the materials.

Materials	Thermal conductivity (W/(m K))	Resistivity (Ω m)	Seebeck coefficient (μV/K)	Young's modulus (GPa)	Poisson's ratio	CTE
Skutterudite (p/n)	2.68–3.62/3.04–4.05	0.62×10^{-5}–0.81×10^{-5}/0.67×10^{-5}–1.17×10^{-5}	92–151.4/−226.5 to −162	110	0.21	0.8×10^{-5}
Bismuth telluride (p/n)	0.82–1.74/0.99–1.99	2.27×10^{-5}–2.94×10^{-5}/0.91×10^{-5}–1.57×10^{-5}	56–230/−161.4 to −120.5	45	0.22	1.6×10^{-5}
Copper conductor	385	1.7×10^{-8}	–	120	0.3	1.7×10^{-5}
Sn–Sb alloy	55	5.0×10^{-8}	–	44.5	0.33	2.7×10^{-5}
Ceramic substrate	25	1.0×10^{12}	–	340	0.22	0.68×10^{-5}

$$\eta = \frac{P}{Q_{in}} \tag{11}$$

The STEG is a kind of irreversible solid state energy conversion device, and its efficiency can also be written as the following form [8],

$$\eta = \frac{T_h - T_c}{T_h} F \tag{12}$$

In which, $T_h - T_c/T_h$ is the efficiency of Carnot cycle. F is a factor related to the operating temperatures and the properties of the component materials ($0 < F < 1$). In the TE system, the power generation cycle is a superposition of an ideal electronic cycle driven by the temperature gradient and electric field force and two irreversible processes. The internal irreversible process relates to the Joule loss and Fourier heat conduction loss through the whole device. And the external irreversible effect is due to the finite rate heat transfer between the device and its heat reservoirs [21]. Although the external heat-resistance losses are not considered, it is seen that, just like any other heat engine, the TE device still runs less efficiently than the ideal Carnot machine due to internal irreversible effects. To analyze the TE behaviors, the load resistance R_0 needs to be determined immediately. Fig. 3 shows the dependences of the output power and conversion efficiency of STEG on the load resistance at hot surface temperature $T_h = 350\ ^\circ C$ and cold surface temperature $T_c = 25\ ^\circ C$ (for convenience, the lengths of the hot segment materials are assumed to be equal, $L_p = L_n$). The maximum output power can be achieved when the load resistance is optimized, that is to say the load resistance is equal to the internal electrical resistance. Since the electrical conductivity of TE materials is temperature-dependent, the internal resistance of the STEG varies with a change in the length of segmented materials. For this reason, the corresponding optimal load resistance are not identical for different segmentation cases. Comparing Fig. 3(a) and (b), it can be found that the optimal load resistance corresponding to the efficiency is different from that with respect to the output power in a given segmentation case. This is mainly because that Q_{in} is also dependent on the load resistance. The conversion efficiency is the most important index to evaluate the TE performance. In order to better capture the effect of the segment on the efficiency, the TE calculation is carried out at a constant load resistance condition. From Fig. 3(b), it can be seen that the peak of the efficiency appears around 14 mΩ. Thus, a load resistance of 14 mΩ is chosen in this study.

Based on the thermal-structure coupling calculation, we can get the thermal stress in STEG under different operating conditions. In this work, the von Mises stress is used to characterize the stress level of the node of the TE material. The maximum allowed stresses

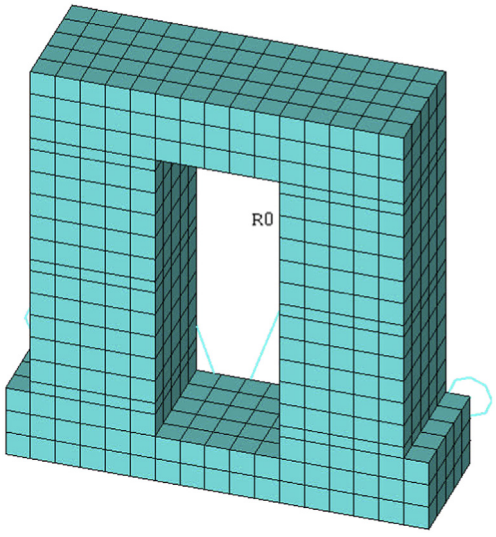

Fig. 2. Finite element model of the STEG.

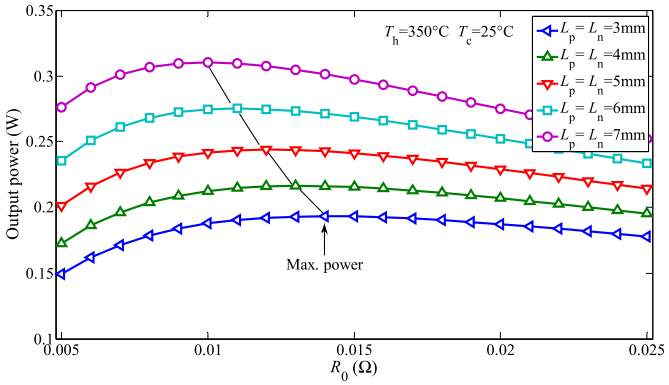

(a) Output power

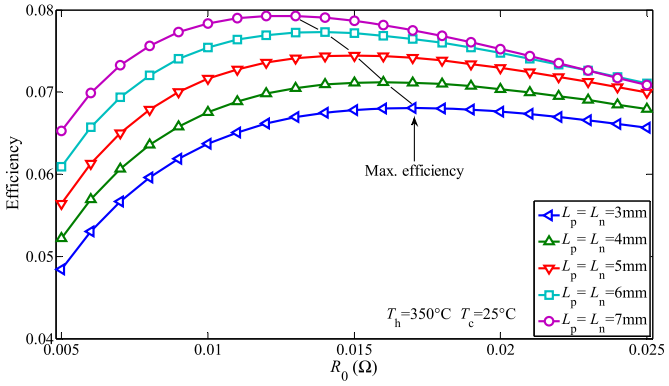

(b) Efficiency

Fig. 3. The variation of the output power and efficiency with the external resistance for various lengths of the hot segment for $T_h = 350\ ^\circ C$ and $T_c = 25\ ^\circ C$.

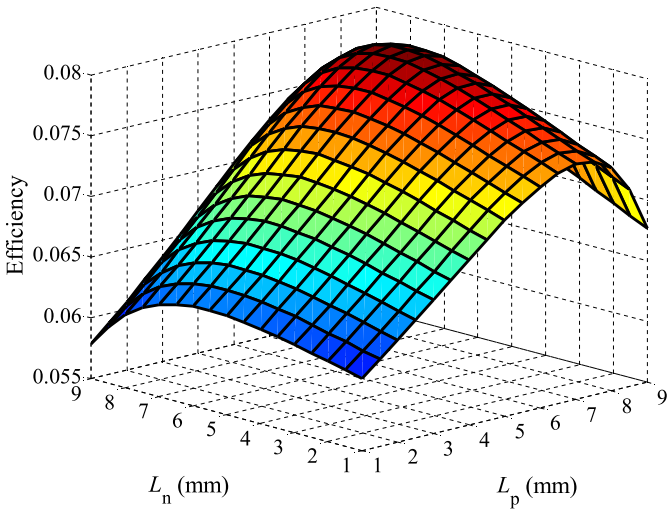

Fig. 4. The variation of the efficiency with the lengths of hot segment materials L_p and L_n for $T_h = 350$ °C and $T_c = 25$ °C.

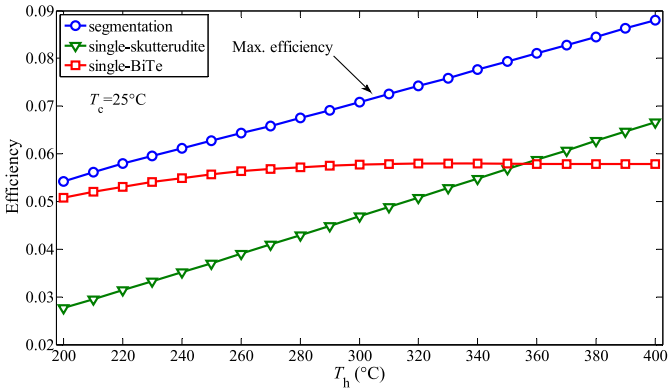

Fig. 5. The variation of the efficiency of the STEG under optimal segmented case, the single-skutterudite and single-BiTe devices with the hot surface temperature T_h.

of the hot segment and cold segment materials are of the order of 100 MPa and 65 MPa, respectively.

3. Results and discussion

Using the above calculation model, we can simulate the thermal-electric and thermal-structure coupling behaviors of the STEG. The rationality and effectiveness of the operating conditions can be verified by the mechanical strength evaluation and mechanical reliability analysis.

3.1. Thermoelectric performance of segmented thermoelectric generators

In order to determine the optimal segmentation scheme, i.e., the one that yields the maximum conversion efficiency, the dependence of the efficiency on the lengths of segmented materials at $T_h = 350$ °C and $T_c = 25$ °C is shown in Fig. 4. The total length of the two TE legs is fixed. And the hot segment lengths (L_p and L_n) are changed from 1 mm to 9 mm. It can be seen that when $L_p = 7.5$ mm and $L_n = 6.5$ mm, the efficiency reaches the maximum value 7.934%. For the standard skutterudite-based and BiTe-based material generators with the same geometry, the efficiency is found to be 5.677% and 5.796%, respectively. One can notice that the STEG shows an increase by 39.8% and 36.9% in efficiency as compared to the standard TE generators. Thus, the theoretical optimal segmentation case is $L_p = 7.5$ mm and $L_n = 6.5$ mm.

For the STEG, in the presence of different operating temperatures, there exit different optimal segmentation schemes. Fig. 5 shows the dependence of efficiency of the STEG for optimal segmentation case with the hot surface temperature (T_h). The efficiencies of the standard generators are also given in this figure. It can be seen that, when the hot surface temperature ranges from 200 °C to 400 °C, the efficiency of the single-skutterudite devices is increasing linearly as the temperature increases. For the single-BiTe devices, when the temperature is relatively low (i.e. $T_h < 300$ °C), the efficiency increases with an increase of temperature. When the temperature is relatively high (i.e. $T_h > 300$ °C), the influence of the temperature on the efficiency is not obvious. This just shows that the BiTe-based TE materials are more suitable for working in low temperature environment. From this figure, it also can be found that the efficiency of the STEG for optimal segmentation case linear change with temperature, and significantly larger than that of single-skutterudite and single-BiTe devices at the same operating temperature. These results prove the fact that the efficiency of TE devices can be enhanced by employing the segmented TE materials.

3.2. Mechanical performance of segmented thermoelectric generators

Excessive thermal stress in TE legs can lead to the TE materials damage which affects the working performance of TE device. Thus, it is very necessary to evaluate the mechanical performance of the STEG. Figs. 6 and 7 describe the thermal stress characteristics in TE

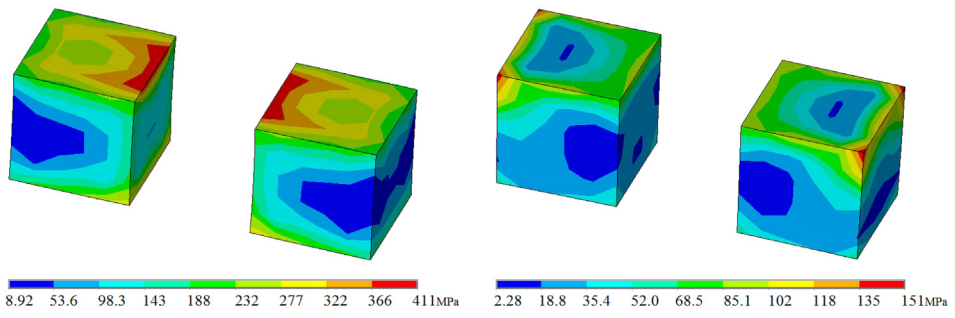

(a) Hot segment (b) Cold segment

Fig. 6. The von Mises stress distributions in segmented TE materials of the STEG with only considering the elastic deformation of the copper strips and the welding strips.

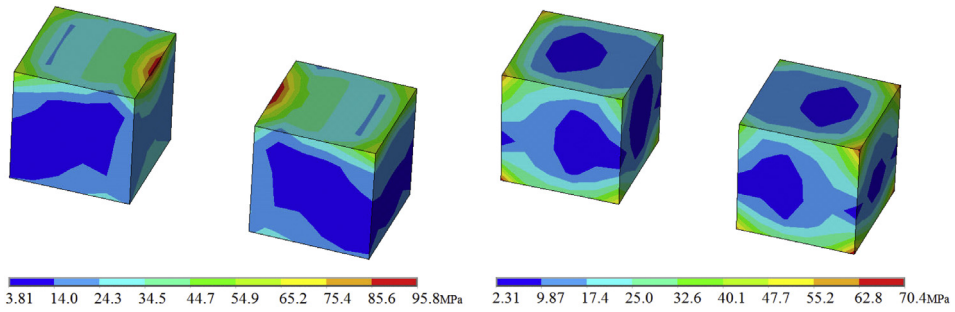

(a) Hot segment (b) Cold segment

Fig. 7. The von Mises stress distributions in segmented TE materials of the STEG with considering the elastoplastic deformation of the copper strips and the welding strips.

materials of the STEG at $T_h = 350$ °C, $T_c = 25$ °C, and $L_p = L_n = 5$ mm. And the elastic stress distribution and the elastoplastic stress distribution are considered, respectively. From Fig. 6, it is found that without considering plastic deformation of the copper strip and welding strip, the maximum Von Mises stress of the hot segment and cold segment materials are 411 MPa and 151 Mpa, respectively. From Fig. 7, we notice that the corresponding values with considering plastic deformation are 95.8 MPa and 70.4 MPa. Obviously, the deformation of the copper strips and welding strips has entered into a plastic stage, and the plastic deformation can effectively moderate the stress level in TE materials. Thus, the plastic behavior cannot be ignored in the thermal-mechanical simulation.

Figs. 8 and 9 show the dependences of the maximum von Mises stress in TE materials on the lengths of the hot segment. From Fig. 8, it can be seen that the change of the maximum stress level in hot segment of p-leg with L_n presents a monotone increasing trend in general. On the contrary, in hot segment of n-leg the stress level is decreasing as the L_n increases. From Fig. 9, we observe that, for the cold segment materials, the stress curves show different characteristics, because the difference of thermal conductivity leads to the different temperature gradient applied to the TE materials. And it is very difficult to figure out the change trends accurately. This is because that the maximum stress level is not always appeared in

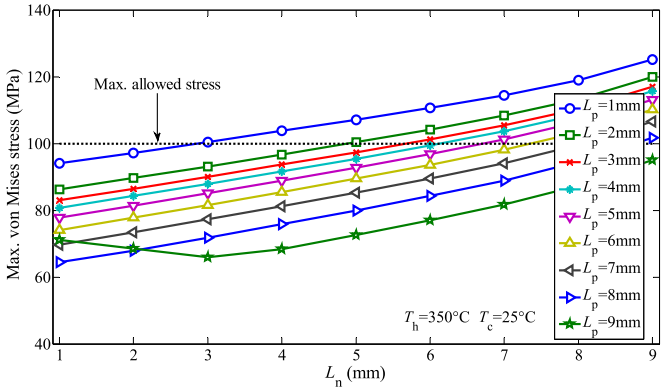

(a) Hot segment of the p-type TE leg

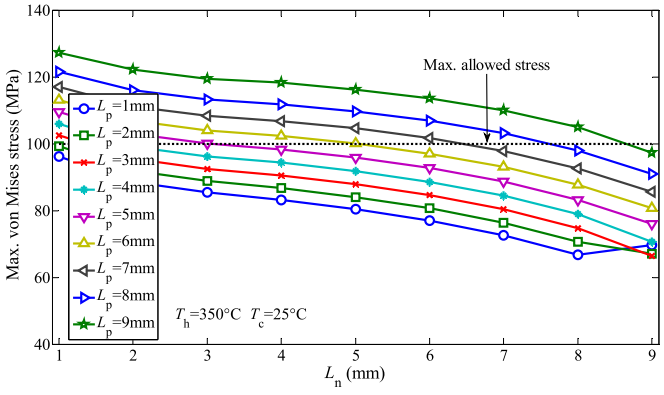

(b) Hot segment of the n-type TE leg

Fig. 8. The variation of the maximum von Mises stress in the hot segment materials with the segment lengths L_p and L_n for $T_h = 350$ °C and $T_c = 25$ °C.

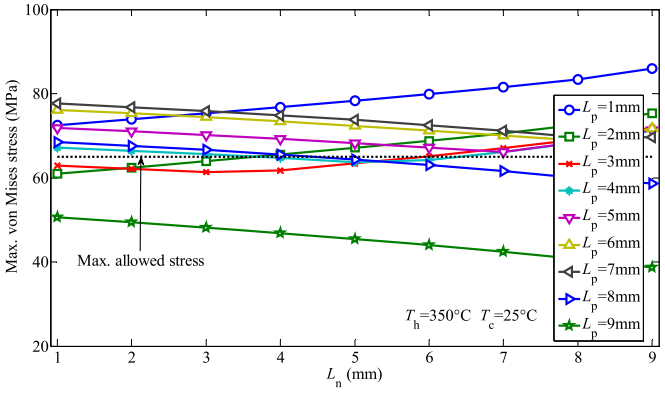

(a) Cold segment of the p-type TE leg

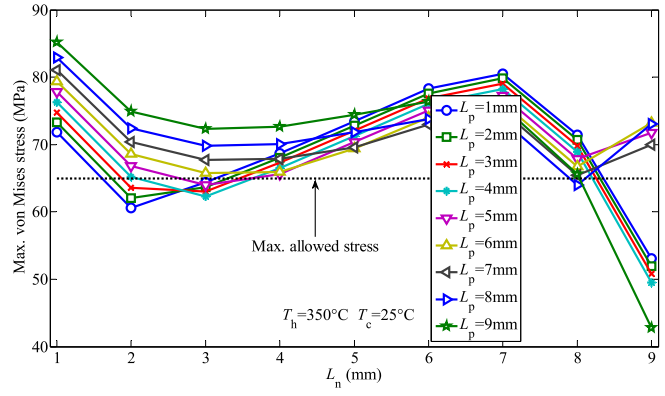

(b) Cold segment of the n-type TE leg

Fig. 9. The variation of the maximum von Mises stress in the cold segment materials with the segment lengths L_p and L_n for $T_h = 350$ °C and $T_c = 25$ °C.

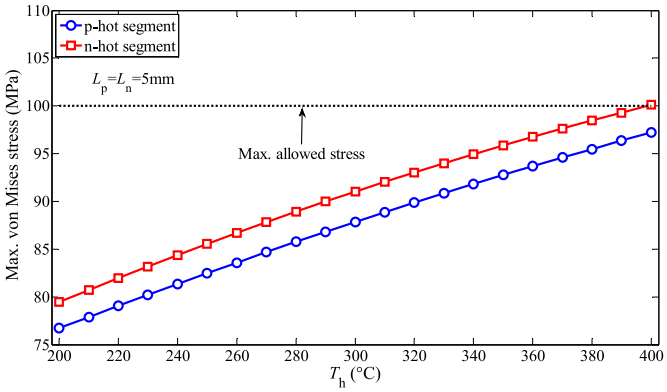

(a) Hot segment

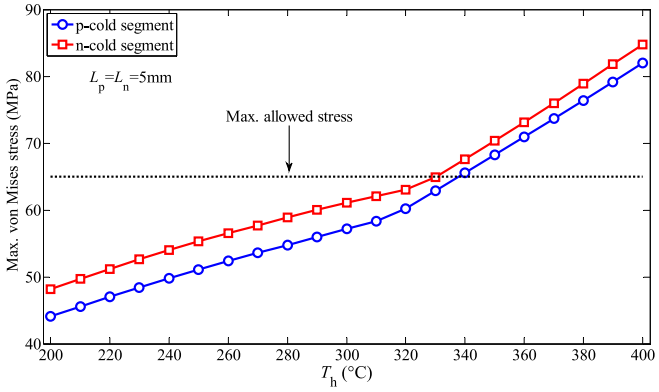

(b) Cold segment

Fig. 10. The variation of the maximum von Mises stress in the segment materials under $L_p = L_n = 5$ mm with the hot surface temperature T_h.

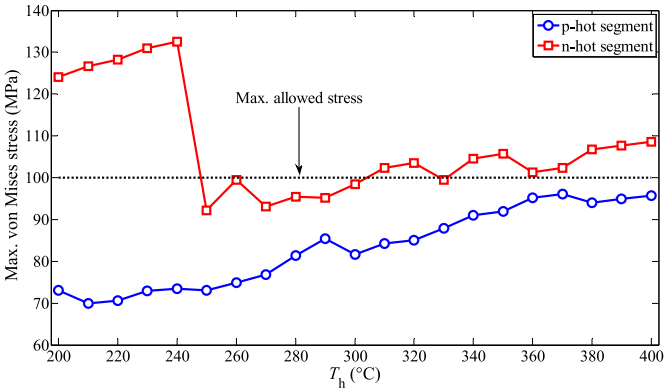

(a) Hot segment

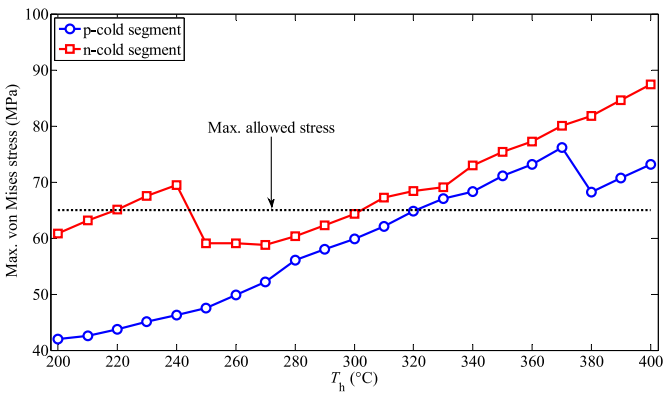

(b) Cold segment

Fig. 11. The variation of the maximum von Mises stress in the segment materials under optimal segmented case with the hot surface temperature T_h.

the same position. It is clearly evident that there are some segmentation cases which do not satisfy the strength requirements.

Then, we discuss the effect of the hot surface temperature on the maximum stress levels in TE materials. Fig. 10 displays the maximum von Mises stresses varying with T_h under a given segmentation case of $L_p = L_n = 5$ mm. It can be found that the maximum stress levels are increasing nonlinearly as the T_h increases. Interestingly, for cold segment BiTe-based materials, the stress curves present an inflection point at $T_h = 320$ °C. This is probably because of the large difference in heat-conduction performance of the BiTe-based material between high temperature and low temperature environments. When $T_h > 330$ °C, the mechanical performance of TE materials no longer satisfies the strength requirements. Fig. 11 displays the maximum von Mises stress in TE materials under optimal segmentation condition. Here, T_h only expresses as the discrete values, and which correspond to different segmentation cases. The maximum stress level is determined by many factors including the hot surface temperature T_h and the segment lengths L_p and L_n. So the variations of the stress with T_h don't follow a certain regulation. It should be noted that some particular temperatures results in the failure of TE materials.

3.3. Optimal operating conditions of segmented thermoelectric generators

For the STEG, the actual optimal operating conditions are determined by balancing the TE and mechanical performances. Under $T_h = 350$ °C and $T_c = 25$ °C, we know that when $L_p = 7.5$ mm and $L_n = 6.5$ mm, the STEG can obtain the maximum conversion efficiency (Fig. 4). In fact, in this case, the maximum stress levels are beyond the maximum allowed stresses of the TE materials (Figs. 8b and 9b), and the security service of the device cannot be guaranteed. With $L_p = L_n = 8$ mm, the STEG can achieve satisfied mechanical and TE performances (Figs. 4, 8 and 9). The corresponding efficiency is 7.183%, and has an increase 37.7% and 34.8% compared with that of single-skutterudite and single-BiTe devices, respectively. This case represents the actual optimal segmentation condition. Within the given temperature ranges, only at 250 °C, 260 °C, 270 °C, 280 °C, 290 °C and 300 °C can the STEG meet the strength requirements of two kinds of TE materials at the same time, and achieve the maximum efficiency (Figs. 5 and 11). These present the actual optimal operating temperatures.

4. Conclusion

This paper develops a 3D finite element model to simulate the TE and mechanical behaviors of segmented thermoelectric generator, and provides a theoretical design guidance for highly reliable and efficient TE devices. The conclusions are as follows:

I. Considering only the high efficiency, the optimal segmentation scheme is $L_p = 7.5$ mm and $L_n = 6.5$ mm. However, such scheme cannot satisfy the strength requirements for TE materials. When $L_p = L_n = 8$ mm, the STEG can achieve satisfied mechanical reliability and conversion efficiency. The corresponding efficiency is still higher than that of the standard single TE material generators. This case presents the actual optimal segmentation condition.

II. For the given temperature ranges, under the theoretical optimal segmentation condition, the efficiency of the device increases linearly with increasing the hot surface temperature T_h, and goes beyond the values of the single TE material devices. The change of the maximum stress level with T_h does not show certain regularity. Only at a few temperatures can the efficiency reach the maximum design value. In addition, the maximum stress level in TE materials with $L_p = L_n = 5$ mm is increasing as the T_h increases.

The results indicate that in contrast to TE devices with homogenous material, the STEG has a better TE performance. In practice, the design for TE devices should balance the maximization of efficiency and the mechanical reliability.

Acknowledgements

The work was supported by grants from the National Natural Science Foundation of China (11372120, 11121202 and 11072093), a grant from the PhD Program Foundation of Ministry of Education of China (20110211110023). The authors would like to express their sincere appreciation to these supports.

Appendix A. Supplementary data

Supplementary data related to this article can be found at http://dx.doi.org/10.1016/j.applthermaleng.2014.07.069.

References

[1] D.M. Rowe, Handbook of Thermoelectrics, CRC Press, Boca Raton, 1995.
[2] F.J. DiSalvo, Thermoelectric cooling and power generation, Science 285 (1999) 703–706.
[3] L.E. Bell, Cooling, heating, generating power, and recovering waste heat with thermoelectric systems, Science 321 (2008) 1457–1461.
[4] Y. Yang, X.J. Wei, J. Liu, Suitability of a thermoelectric power generator for implantable medical electronic devices, J. Phys. D Appl. Phys. 40 (2007) 5790–5800.
[5] B. Jang, S. Han, J.Y. Kim, Optimal design for micro-thermoelectric generators using finite element analysis, Microelectron. Eng. 88 (2011) 775–778.
[6] A.Z. Sahin, B.S. Yilbas, The thermoelement as thermoelectric power generator: effect of leg geometry on the efficiency and power generation, Energy Convers. Manag. 65 (2013) 26–32.
[7] L.G. Chen, J. Li, F.R. Sun, C. Wu, Performance optimization for a two-stage thermoelectric semiconductor thermoelectric-generator, Appl. Energy 82 (2008) 300–312.
[8] V.L. Kuznetsov, L.A. Kuznetsova, A.E. Kaliazin, D.M. Rowe, High performance functionally graded and segmented Bi_2Te_3-based materials for thermoelectric power generation, J. Mater. Sci. 37 (2002) 2893–2897.
[9] L.N. Vikhor, L.I. Anatychuk, Generator modules of segmented thermoelements, Energy Convers. Manag. 50 (2009) 2366–2372.
[10] B.V.K. Reddy, M. Barry, J. Li, M.K. Chyu, Mathematical modeling and numerical characterization of composite thermoelectric devices, Int. J. Therm. Sci. 67 (2013) 53–63.
[11] Th Clin, S. Turenne, D. Vasilevskiy, R.A. Masut, Numerical simulation of the thermoelectrical behavior of extruded bismuth telluride alloy module, J. Electron. Mater. 38 (7) (2009) 994–1001.
[12] S. Turenne, Th. Clin, D. Vasilevskiy, R.A. Masut, Finite element thermo-mechanical modeling of large area thermoelectric generators based on bismuth telluride alloys, J. Electron. Mater. 39 (9) (2010) 1926–1933.
[13] A.S. Al-Merbati, B.S. Yilbas, A.Z. Sahin, Thermodynamics and thermal stress analysis of thermoelectric power generator: influence of pin geometry on device performance, Appl. Therm. Eng. 50 (2013) 683–692.
[14] S.L. Li, C.K. Liu, C.Y. Hsu, M.C. Hsieh, M.J. Dai, S.T. Wu, Thermo-mechanical analysis of thermoelectric modules, in: Microsystems Packaging Assembly and Circuit Technology Conference, Proceedings, 2010, pp. 1–4.
[15] G. Chen, Y. Mu, P.C. Zhai, G.D. Li, Q.J. Zhang, An investigation on the coupled thermal-mechanical-electrical response of automobile thermoelectric materials and devices, J. Electron. Mater. 42 (7) (2013) 1762–1770.
[16] J.L. Gao, Q.G. Du, X.D. Zhang, X.Q. Jiang, Thermal stress analysis and structure parameter selection for a Bi_2Te_3-based thermoelectric module, J. Electron. Mater. 40 (5) (2011) 884–888.
[17] E.E. Antonova, D.C. Looman, Finite elements for thermoelectric device analysis in ANSYS, in: Proc. Int. Conference on Thermoelectrics, Proceedings, 2006, pp. 200–203.
[18] J.F. Nye, Physical Properties of Crystals: Their Representation by Tensors and Materials, Oxford University Press, New York, 1985.
[19] P. Ziolkowski, P. Poinas, J. Leszczynski, G. Karpinski, E. Müller, Estimation of thermoelectric generator performance by finite element modeling, J. Electron. Mater. 39 (9) (2010) 1934–1943.
[20] D. Ebling, M. Jaegle, M. Bartel, A. Jacquot, H. Böttner, Multiphysics simulation of thermoelectric systems for comparison with experimental device performance, J. Electron. Mater. 38 (7) (2009) 1456–1461.
[21] L.G. Chen, F.R. Sun, C. Wu, Thermoelectric-generator with linear phenomenological heat-transfer law, Appl. Energy 81 (2005) 358–364.